

## Durham E-Theses

---

*Analysis of the strong field approximation for  
harmonic generation and multiphoton ionization in  
intense ultrashort laser pulses*

Ciprian Constantin Chirilă

### How to cite:

---

Chirilă, Ciprian Constantin (2004) Analysis of the strong field approximation for harmonic generation and multiphoton ionization in intense ultrashort laser pulses. Doctoral thesis, Durham University.

### Use policy

---

The full-text may be used and/or reproduced, and given to third parties in any format or medium, without prior permission or charge, for personal research or study, educational, or not-for-profit purposes provided that:

- a full bibliographic reference is made to the original source
- a <https://etheses.durham.ac.uk/id/eprint/10633/> is made to the metadata record in Durham E-Theses
- the full-text is not changed in any way

The full-text must not be sold in any format or medium without the formal permission of the copyright holders.

Please consult the [full Durham E-Theses policy](#) for further details.

# Chapter 6

## Direct ionization in short pulses

### 6.1 Outline

In this chapter, we present the predictions of the Coulomb-corrected SFA model (KSFA) for direct ionization in short laser pulses. We show that the model confirms the well-known sensitivity of the angle-resolved ATI energy spectra to the absolute phase. This is also the case in the context of harmonic generation [94, 95]. The origin of this can be traced to the interplay between electron trajectories corresponding to direct ionization in the Simpleman's model. Finally, total probabilities are calculated and compared to those obtained using the exact static rates or the tunneling rate. The relevance of the Keldysh adiabaticity parameter  $\gamma$  is discussed. For all the cases studied here, we are in the tunneling regime, i.e.,  $\gamma < 1$ , unless otherwise stated, and the laser intensity is such that the ionization is not in the over-the-barrier regime for the atomic systems considered.

In the last part of the chapter, we compare the predictions of the Coulomb-corrected SFA model to the fully numerical results from the Schrödinger equation; the major differences and their possible explanations are emphasized.

## 6.2 Pulse form and classical energy cutoffs

At relatively small intensities, the dipole approximation can be invoked. The magnetic field component of the pulse accelerates the electrons in the direction of field propagation for a linearly polarized laser, which tends to suppress re-collision processes. At 800 nm, the wavelength of a Ti:Sapphire laser, this effect becomes non-negligible for intensities above  $10^{17}$  W/cm<sup>2</sup>, in which case a non-dipole description is necessary.

Using the dipole approximation, the response of the atom to a linearly polarized laser pulse can be calculated by taking an electric field  $\mathbf{E}(t) = E(t)\hat{\mathbf{e}}$  and a vector potential  $\mathbf{A}(t) = A(t)\hat{\mathbf{e}}$ . Although in some cases accurate numerical representations of the pulse are necessary, a simple analytical model is adequate in many applications. Assuming no chirp (the frequency is constant for the pulse), one can adopt the simple expression

$$E(t) = E_0 \chi(t) \sin(\omega t + \phi),$$

for the electric field of the pulse, or, alternatively,

$$A(t) = E_0/\omega \chi(t) \cos(\omega t + \phi)$$

for the pulse's vector potential. The two approximations are equivalent provided that the pulse is sufficiently long for  $d\chi/dt$  to be negligible compared to  $\omega\chi(t)$ . It is convenient to characterize the pulse intensity by the peak intensity,  $I_0$ , defined as for the stationary field,  $I_0 = E_0^2/2$ , assuming that  $0 \leq \chi(t) \leq 1$ .

The envelope function,  $\chi(t)$ , is usually taken a half-period  $\sin^2$  function, encompassing a certain number of cycles  $n$ , such that

$$A(t) = A_0 \sin(\omega t + \phi) \sin^2(\omega t/2n). \quad (6.1)$$

In this case, the pulse has a strictly finite duration. If we define the full width at half maximum (*FWHM*) as the time interval during which the intensity envelope is bigger than half the peak intensity  $I_0$ , we obtain for the  $\sin^2$  pulse

$FWHM = 4n \arccos(2^{-1/4})/\omega$ , or, in terms of one optical period  $T = 2\pi/\omega$ ,  $FWHM/T = 2n \arccos(2^{-1/4})/\pi \approx 0.364n$ . If instead of intensity, we choose the field amplitude, then  $FWHM = n\pi/\omega$ , or  $FWHM/T = n/2$  field periods.

Other popular choices are a Gaussian function (which is convenient as the intensity drops fast in the wings, but perhaps not as good a representation of the actual pulse) and a sech function. The later has for the vector potential

$$A(t) = A_0 \sin(\omega t + \phi) \operatorname{sech}(\omega t/\tau), \quad (6.2)$$

and the full width at half maximum in intensity is  $FWHM = 2\tau \operatorname{arccosh}\sqrt{2}/\omega$  or, in units of one optical cycle,  $FWHM/T = \tau \operatorname{arccosh}\sqrt{2}/\pi \approx 0.281\tau$ . In amplitude,  $FWHM = 2\tau \operatorname{arccosh}2/\omega$ , or  $FWHM/T = \tau \operatorname{arccosh}2/\pi \approx 0.419\tau$  optical cycles. Figure 6.1 shows a  $\sin^2$  and a sech pulse with identical FWHM.

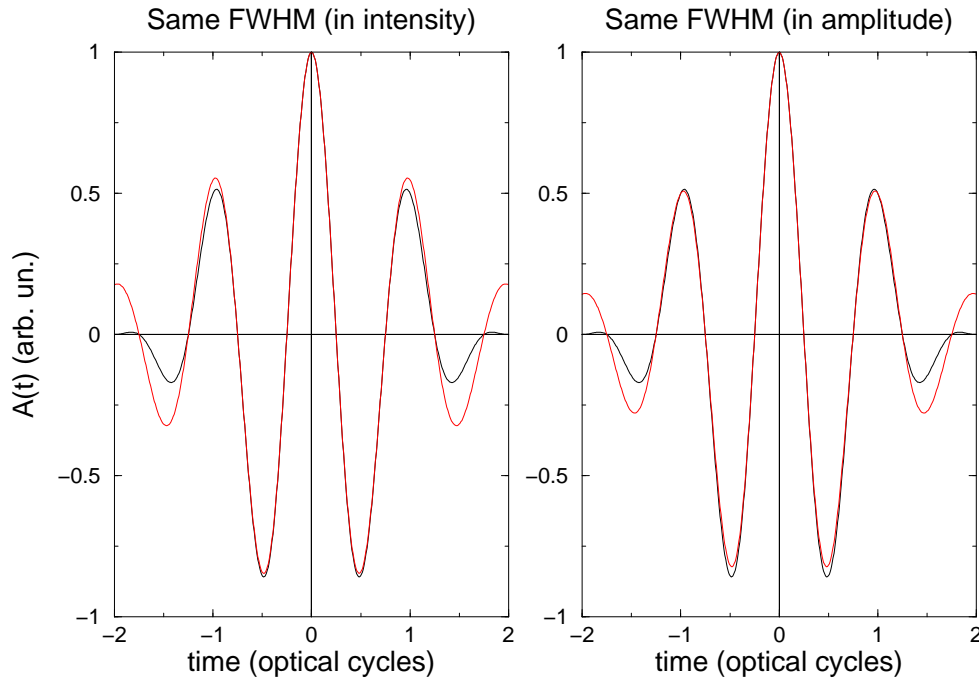


Figure 6.1: Left panel: a 4-cycle  $\sin^2$  pulse (black curve) and a sech pulse (red curve) with the same FWHM (in intensity). The phase is  $\phi = \pi/2$ . The right panel shows the same, only for identical FWHM in amplitude.

To give an idea about the changes one might expect in the case of short pulses

when compared to a stationary field, we calculate the maximal kinetic energy at the time of return  $t$  of an electron starting in the origin at a time  $t'$  during the pulse, as well as the maximum kinetic energy after rescattering. If we define the quantity  $k_s(t, t') = -\int_{t'}^t A(\tau) d\tau / (t - t')$ , we look for the pair of ‘birth’ time  $t'$  and return time  $t$  (as in the Simpleman’s model) for which the return kinetic energy  $E_{ret} = [A(t) - A(t')]^2/2$  is maximal, or the rescattering kinetic energy  $E_{res} = [2A(t) - A(t')]^2/2$  is maximal. The solution must satisfy the condition  $k_s(t, t') + A(t') = 0$ , which means that the electron is back at the origin at time  $t$ . For the stationary field we have the well known values of  $E_{ret} = 3.1731 U_p$  and  $E_{res} = 10.0076 U_p$ , with  $U_p$  the ponderomotive energy  $U_p = A_0^2/4$ .

Figure 6.2 shows the maximal return and rescattering energies in units of the ponderomotive potential  $U_p$  for a  $\sin^2$  pulse with  $A(t) \propto \sin(\omega t) \sin^2(\omega t/2n)$ , as a function of the number of optical cycles  $n$ . The convergence to the values

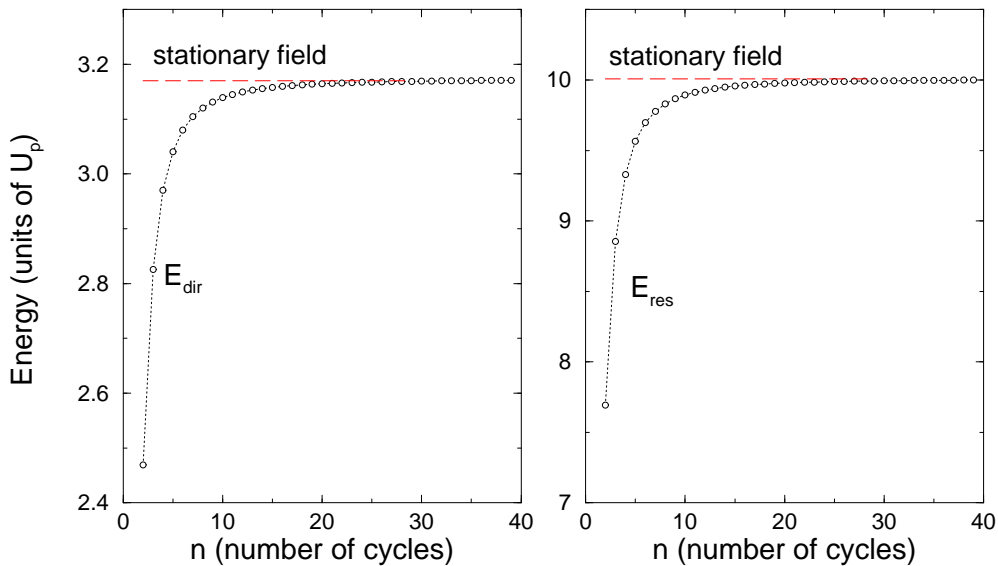


Figure 6.2: The cutoffs for the return (left panel) and rescattering (right panel) kinetic energy for a  $n$ -cycle  $\sin^2$  pulse, with  $A(t) \propto \sin(\omega t) \sin^2(\omega t/2n)$ .

for the stationary field is readily achieved for both the direct and rescattering maximal energies. This shows that the envelope of the field can affect to a certain extent the physical processes. Some particular values are given in

Table 6.1; it is easy to see that already for a pulse with 38 optical cycles, the direct cutoff agrees to the stationary field's value with 0.07% relative accuracy.

$n$	2	4	5	10	14	19	28	38
$E_{dir}/U_p$	2.469	2.970	3.040	3.139	3.156	3.164	3.169	3.171
$E_{res}/U_p$	7.693	9.330	9.565	9.893	9.949	9.976	9.992	9.999

Table 6.1: Cutoffs for return and rescattering energy for  $\sin^2$  pulses with different number of cycles (see Fig. 6.2).

Figure 6.3 shows the dependence with the phase  $\phi$  of both energy cutoffs, for a 4-cycle pulse. The variation in the cutoff energies can be steep for certain values of  $\phi$ . On the basis of the Simpleman's model, this indicates that the ionization process is highly sensitive to the phase of the field. Also, it points out that the relative phase  $\phi$  can influence the process to a great extent, and it is important in applications to be able to produce laser pulses with controllable absolute phase and to find ways to accurately measure it.

### 6.3 Definitions of SFA angular and energy distributions

We use the Krainov Coulomb-corrected ionization amplitude [Eq. (5.22)], while for the vector potential we choose a linearly polarized field along the axis  $\epsilon$ , with  $\mathbf{A}(t) = A_0 \sin(\omega t + \phi) \sin^2(\omega t/2n) \hat{\epsilon}$ . Choosing the vector potential zero at the beginning and the end of the pulse gives numerical advantages when calculating the transition amplitudes, by avoiding the boundary terms affecting the physical result. The quantities of interest are:

- the differential ionization probability for the emission of an electron with energy  $E_p \equiv \mathbf{p}^2/2 = kU_p$  in the direction  $\theta$  with respect to the polarization axis:

$$w(\theta, \phi) = \frac{|M_{\mathbf{p}}^{(0)}|^2 d^3\mathbf{p}}{d\Omega_{\mathbf{p}} dk} = U_p \sqrt{2kU_p} |M_{\mathbf{p}}^{(0)}|^2, \quad (6.3)$$

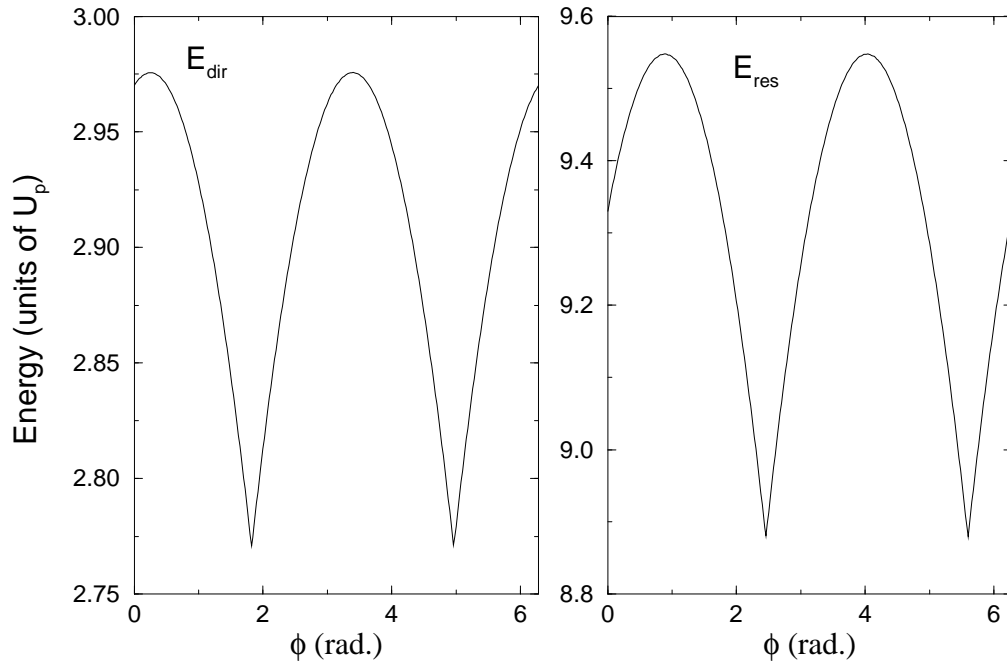


Figure 6.3: The phase dependence of the maximal return (left panel) and rescattering (right panel) kinetic energy for a 4-cycle  $\sin^2$  pulse, with  $A(t) \propto \sin(\omega t + \phi) \sin^2(\omega t/8)$ .

where  $\phi$  is the polar angle of the electron's asymptotic momentum in a plane perpendicular to the polarization direction and  $\theta$  is the angle of ejection with respect to the polarization direction;  $M_{\mathbf{p}}^{(0)}$  is the Krainov's transition amplitude for direct ionization. The electron emission is symmetrical around the polarization direction of the field (namely, the same for any value of  $\phi$ );

- the differential probability per unit energy (in units of  $U_p$ ) and per unit azimuthal angle  $\theta$ , integrated over the polar angle  $\phi$ :

$$w(k, \theta) \equiv \frac{d^2\mathcal{P}}{dk d\theta} = 2\pi \sin \theta U_p \sqrt{2kU_p} |M_{\mathbf{p}}^{(0)}|^2, \quad (6.4)$$

with  $E_p \equiv \mathbf{p}^2/2 = kU_p$ .

Both distributions, integrated over the emission angles and energies, give the total emission probability. The angle/energy integrated probability is given by

the integration of Eq. (6.4) over  $\theta$  and  $k$ , respectively:

$$\frac{d\mathcal{P}}{dk} = \int_0^\pi w(k, \theta) d\theta$$

and

$$\frac{d\mathcal{P}}{d\theta} = \int_0^\infty w(k, \theta) dk.$$

## 6.4 The accuracy of the saddle point method

Before presenting numerical results obtained for energy distributions of the ejected electrons in the case of finite laser pulses, we discuss first the accuracy of the saddle point method.

As discussed in detail in Appendix E.2.2, the exact integration can be performed in two ways: (i) Along the real axis, by using a special method to deal with the strongly oscillatory behavior of the integrand or (ii) Along a path in the complex plane, passing through the saddle point closest to the real axis, and connected to the end points of the integration interval by vertical lines. Of course, the results obtained by using either of the methods are identical in view of the Cauchy theorem.

Nonetheless, the complex plane integration method intuitively reveals a result from the asymptotic theory: the main contributions to an integral come from its saddle points (the integrand decreases exponentially in their vicinity) and from the end points of the integration interval. The latter part is known as the ‘boundary contribution’ and can be calculated analytically as an infinite series involving derivatives of the integrand, calculated at the end points (for more details, see Subsection E.2.2). In practice, we use only the first order boundary term (BT) contribution as the expressions for higher orders become increasingly cumbersome.

The BT terms can be shown to depend on the derivatives of the electric field at the beginning and the end of the laser pulse, i.e., on the way the laser

pulse is switched on and off. If the electric field derivatives at the temporal boundaries of the pulse are not negligible, then their inclusion in the result will distort the ionization spectrum. Therefore, according to one's intuition, the BT contribution should be extracted from the integral giving the ionization amplitude.

A way to eliminate the BT is to perform the calculation in the complex plane, and taking as a final result only the contribution coming from the path that goes through the saddle point, parallel to the real axis. The contributions coming from the connection paths with the end points of the integration interval should be thus discarded, as they represent the BT contribution. The result of such a procedure should be approximated to a high accuracy by the contribution of the saddle points. We show that this is indeed the case for the laser parameters we use. This way, the saddle point calculation implicitly discards the BT contribution and gives correct physical results.

Another way is to perform the calculation along the real axis and subtract the first order BT contribution only. The results agrees to the saddle point contribution, provided the higher order BT are negligible, which happens if the electric field is a smooth function at the beginning and the end of the pulse, or if the pulse is long enough (see Appendix E.2.2 for more details).

To illustrate the above, we present two sets of results: one for angle-resolved ATI energy spectra and the other for angular distribution of the ejected electron.

Figure 6.4 shows in the left panel an angle-resolved ATI energy spectrum for low field intensity, where BT are expected to play a role. Calculating the ionization amplitude by integration along the real axis followed by subtraction of the first order BT (red curve) is compared to the result obtained by integrating along the path in the complex plane, parallel to the real axis and going through the saddle point (hence eliminating the BT contribution – black curve). (The complex path integration agrees well with the result of the saddle

point method, as expected; the two cannot be distinguished on the scale of the graph.) Although the first order BT is extracted, there is a clear difference, due to higher order BT. For higher intensity (right panel), the two calculations (the saddle point and the one from which the first order BT has been subtracted) yield results in excellent agreement, undistinguishable on the scale of the graph. Should the BT terms not have been extracted from the integration along the real axis, we would obtain a result of order  $10^3$  a.u. instead of  $10^{-8}$  in the left panel of Figure 6.4.

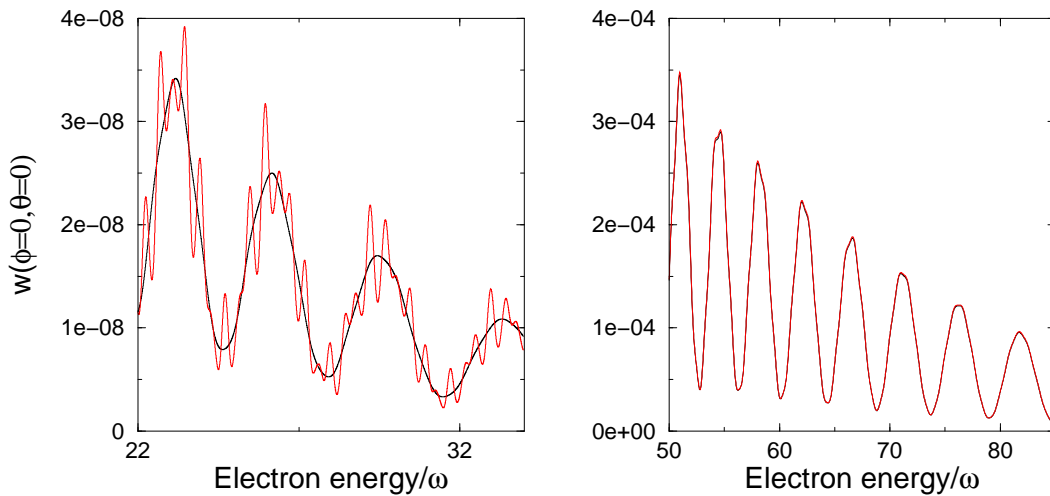


Figure 6.4: Angle-resolved [Eq. (6.3)] ATI energy spectra for electron emission from  $\text{He}^+$  along the polarization axis for an electric field amplitude  $E_0 = 0.2$  a.u. (left panel) and  $E_0 = 0.3$  a.u. (right panel). The wavelength is 800 nm and the pulse duration is four optical cycles with  $\phi = 0$ . The red curves show the exact integration result from which the first order boundary term (BT) has been subtracted and the black curves show the saddle point result.

Similar comments can be made for the case of angular distribution spectra. The same values for intensities as in Fig. 6.4 are chosen in Fig. 6.5 for angular distribution spectra. The quantitative agreement with the saddle point results become better for higher intensity and/or for longer pulses.

In conclusion, for the range of intensities we are interested in, the saddle point method provides accurate numerical results for the ionization amplitudes. As the method is fast, it enables us to calculate, in a reasonable amount of com-

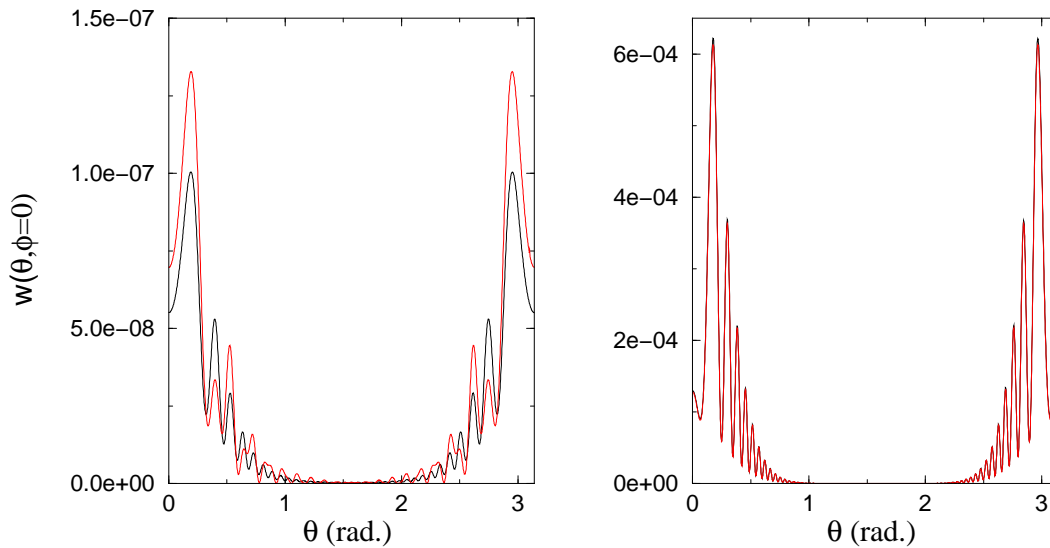


Figure 6.5: Angular distributions in  $\text{He}^+$  for electron energy of  $0.1U_p$ . The pulse parameters are the same as in Fig. 6.4. The red curves show the exact integration result from which the first order boundary term (BT) has been subtracted and the black curves show the saddle point result.

putational time, angle/energy-integrated spectra or total probabilities.

## 6.5 Total ionization probabilities

The usual SFA model includes the Coulomb interaction in a first step, by using the exact wavefunction for the initial bound state of the ionizing electron. Further improvements include corrections due to tunneling through the potential barrier formed by the Coulomb potential and the external field: one way to do this is given by the KSFA version we use in our calculations. The accuracy for taking into account the Coulomb interaction within the SFA proved to be sufficient for obtaining correct total probabilities of ionization [37, 87, 89, 96].

In this section, we analyze the results for the ionization probabilities in a short laser pulse, given by the SFA model (with and without Coulomb correction). These are compared to the approximate results obtained by integrating along the pulse duration the exact ionization rate for a constant electric field; this

way, due to the low frequency of the carrier wave, we implicitly assume that the ionization process is of adiabatic nature. The ion studied is  $\text{He}^+$ .

The total ionization probability is calculated by integrating Eq. (6.3) or (6.4) over the ejection angle and energy. For a 4-cycle,  $\sin^2$  pulse with zero phase, the dependence with the laser peak intensity of the ionization probability calculated within the Coulomb-corrected SFA model is given by the blue curve in Fig. 6.6. In contrast to the results predicted by the usual SFA (for which the difference can be as much as two orders of magnitude), the Coulomb-corrected results are much closer to the estimated probabilities from the integration of the exact static rates (red curve). This justifies the use of the Coulomb-corrected SFA as a way to get more accurate quantitative results. As it will be shown in the next section, there are still significant qualitative differences between the Coulomb-corrected version and the exact results, but the order of magnitude is the same.

As seen in the similar comparison made for the stationary field, for higher intensities (thus lower Keldysh adiabaticity factor), the Coulomb-corrected SFA gives results closer to the ones obtained from integration of the static tunneling ionization rate of Landau and Lifshitz. Knowing the rate of ionization for a constant field  $\Gamma(E)$ , one can calculate the ionization probability as  $\mathcal{P} = 1 - \int_0^{T_p} \Gamma[E(t)]dt$ , where the integration is done over the entire laser pulse. The agreement at low Keldysh adiabaticity parameters comes from the proven fact that the rate of ionization obtained from the Coulomb-corrected SFA goes in the low frequency limit into exactly the static ionization rate (see Appendix D).

To conclude, the Coulomb-corrected SFA model gives results that are in better agreement with the adiabatic estimates of the ionization probabilities, than those of the usual SFA model. In the limit of low Keldysh adiabaticity parameter, the Coulomb-corrected SFA is close to the results coming from the integration of the static ionization rates. This proves that for the case examined here, in the tunneling limit, the ionization process is to a good approximation,

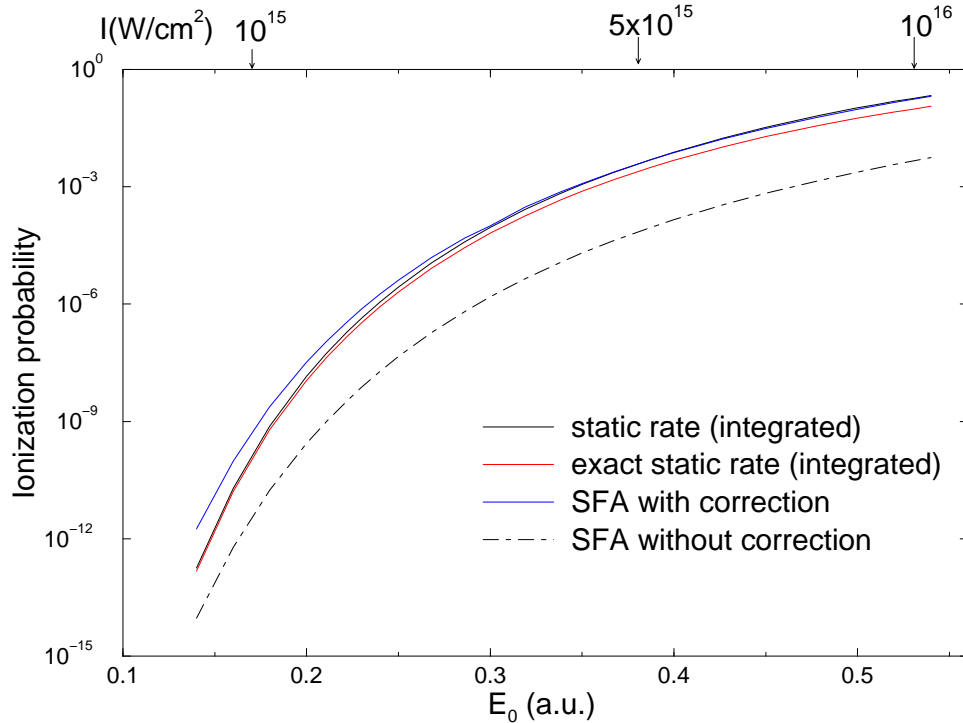


Figure 6.6: Total ionization probability for a  $\text{He}^+$  ion irradiated by a four-cycle  $\sin^2$  pulse, with  $\phi = 0$ . The results are given as a function of the peak intensity and originate for the usual and KSFA model. The other two estimates were calculated using the exact rate of ionization in a static electric field and the Landau and Lifshitz static tunneling rate, respectively.

adiabatic. As a final remark, the corrected SFA proves to be a useful tool to obtain estimates of the ionization probabilities in short laser pulses.

In the next section, we discuss the agreement of the Coulomb-corrected SFA with *ab initio* results, analyzing in detail some ATI angular distributions.

## 6.6 Differential ionization probabilities

We present some predictions of the Krainov Coulomb-corrected SFA model (KSFA) for direct ionization in short pulses, in the case of various ions. In Section 6.10 we show that for the field parameters and the atomic system studied there, the model is able to reproduce qualitatively the general charac-

teristics of the ATI spectra and predicts emission probability of the same order of magnitude as the results obtained from the Schrödinger equation (Section 6.10). The interference effects met in the case of the stationary field cannot build up unless the pulse is long enough. Without the Krainov correction, the SFA in the length gauge or velocity gauge predicts results that are a few orders of magnitude lower than the *ab initio* results.

Figure 6.7 shows the differential ionization probability [Eq. (6.4)] for two emission angles, close to the the axis of polarization. One remarkable feature is

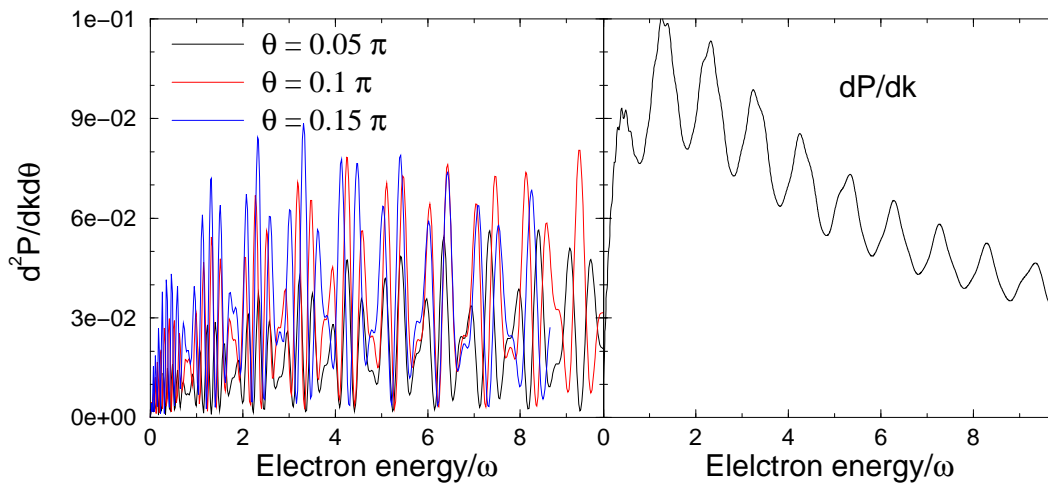


Figure 6.7: Left panel: angle-resolved ATI spectra for different emission angles  $\theta$  with respect to the polarization direction. Right panel: angle-integrated ATI spectra. The pulse is with a  $\sin^2$  envelope, encompassing four optical cycles, with 800 nm wavelength. The electric field amplitude is  $E_0 = 0.4$  a.u. The ion is  $\text{He}^+$ .

that for low ATI orders (LATI), the peaks occur at approximately the same energies, irrespective of the angle of emission. As a result, when integrating the probability over the emission angle, the LATI are still present in the angle-integrated spectrum (see the right panel of Fig. 6.7). As explained below, the weak dependence of LATI on emission angle is linked to the fact that the field phase  $\phi$  is zero in Eq. (6.1). (The electric field is symmetrical with respect to the middle of the pulse.)

For a field phase different from zero, LATI peaks become less and less resolved

in the angle-integrated spectrum, until they eventually disappear. Figure 6.8 shows the case when the electric field is anti-symmetrical with respect to the middle of the pulse [ $\phi = \pi/2$  in Eq. (6.1)]. The energies of the LATI peaks

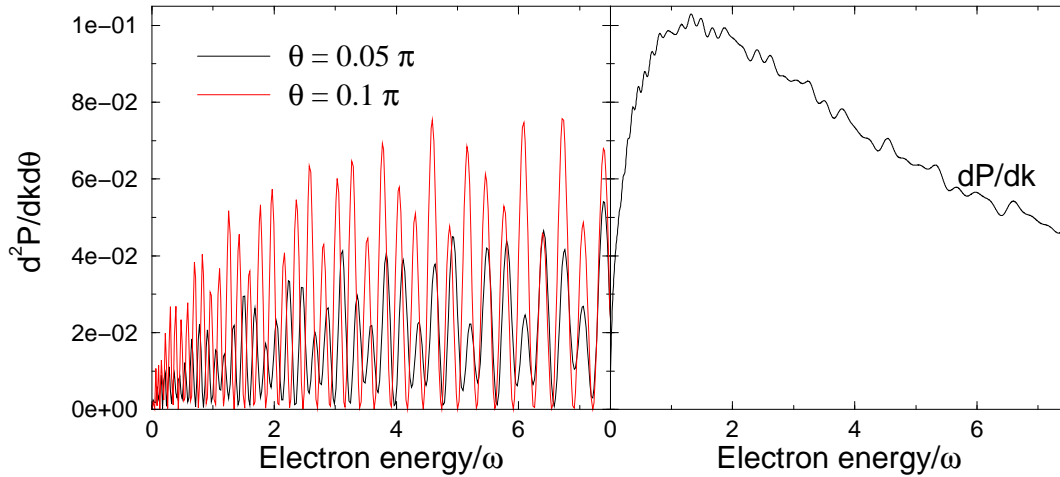


Figure 6.8: Left panel: angle-resolved ATI spectra for different emission angles  $\theta$  with respect to the polarization direction. Right panel: angle-integrated ATI spectra. The parameters are the same as in Fig. 6.7, only the field phase is changed:  $\phi = \pi/2$

depend now on the emission angle as it can be seen in the left panel. Hence, integrating over the angle of emission  $\theta$  smoothes the spectrum, leading to less resolved LATI peaks. In particular, for the anti-symmetrical electric field, there are no peaks in the angle-integrated ATI spectrum, as the right panel of Fig. 6.8 shows. This dependence of LATI peaks on the field phase could help measuring the absolute phase of a short laser pulse.

Figure 6.9 shows the differential probability for two energies of the ejected electron, as a function of the emission angle  $\theta$ . Note the decrease for higher energies although their values are far below the cutoff value. The probability of emission decreases faster for electrons not ejected along the polarization direction (which corresponds to  $\theta = 0$  and  $\theta = \pi$ ). For high ejection energies, the emission perpendicular to the polarization axis is practically negligible, this being characteristic for ionization in linearly polarized radiation. The dashed curves in Fig. 6.9 show the energy-integrated probability. Because

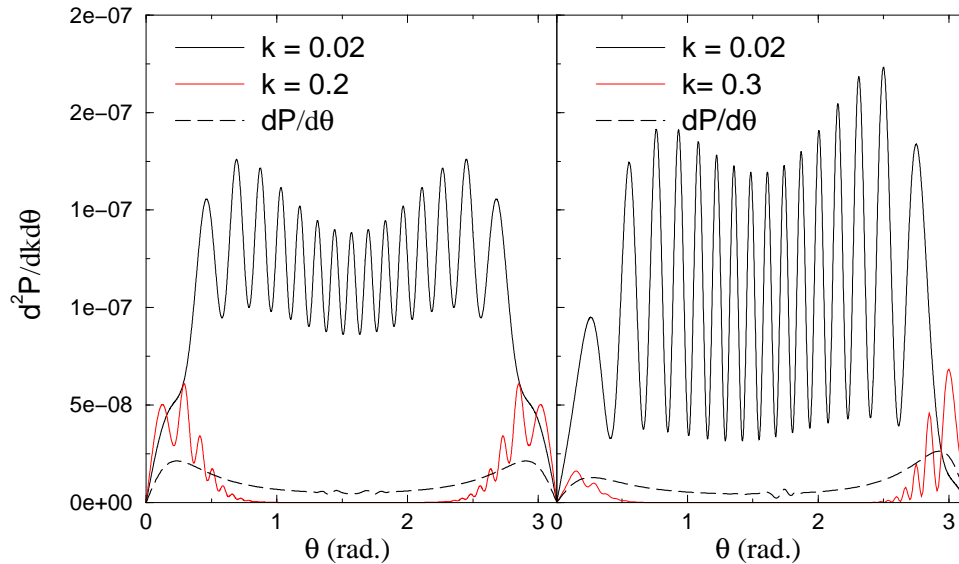


Figure 6.9: The differential ionization probability for constant electron energy as a function of the emission angle and the energy-integrated probability for  $\text{He}^+$  irradiated by a four-cycle  $\sin^2$  pulse with peak electric field  $E_0 = 0.2$  a.u. Left panel: the field phase is  $\phi = 0$ , right panel:  $\phi = \pi/4$ . The wavelength is 800 nm. (The ponderomotive energy is  $U_p = 0.77$  a.u.)

of the symmetrical electric field with respect to the middle of the pulse, the electron emission in the left panel has a backward-forward symmetry (i.e., emission at angle  $\theta$  is the same as for the angle  $\pi - \theta$ ). This is typical to Keldysh-like theories as the Coulomb interaction, responsible for breaking the symmetry, is not included. (For a more detailed discussion of Keldysh-like theories for ionization in elliptical polarization, see Ref. [97] or for asymmetries in short laser pulses see Ref. [98].) Another symmetry is for rotations around the polarization axis; together with the other symmetry, it gives the known fourfold symmetry of the angular distribution of the SFA model. The right panel of the same figure depicts the case of a nonzero value of the field phase. As the electric field is not symmetrical with respect to the middle of the pulse, the electron emission is bigger in that direction of the polarization axis in which the electric field points mostly during the pulse. This effect is discussed in Section 6.9.

## 6.7 Mathematical analysis

Based on the saddle point method, the interference effects due to different electron trajectories during the pulse duration can be analyzed and, for low energies, approximate analytical expressions describing this interference can be found.

The ionization amplitude is given by a sum over the contribution of all saddle points, of the form:

$$\mathcal{A} = \sum_{l=1}^{n_s} a_l \exp(iS_l), \quad (6.5)$$

where  $a_l$  and  $S_l$  are the amplitudes and the phase of the contribution of saddle time  $t_l$ . The modulus squared reads:

$$|\mathcal{A}|^2 = \sum_{l=1}^{n_s} a_l^2 + 2 \sum_{\substack{l, m=1 \\ m>l}}^{n_s} a_l a_m \cos(S_l - S_m), \quad (6.6)$$

In order to analyze the possible interference effects in Eq. (6.6), one needs to calculate the expression of the phase difference between any two saddles. The saddle points are solutions of the equation  $[\mathbf{p} + \mathbf{A}(t)]^2/2 + I_p = 0$ ; the equation can be re-written as  $A(t_s) = -p_{\parallel} \pm i\sqrt{2I_p + p_{\perp}^2}$ , where the indices for the asymptotic momentum  $\mathbf{p}$  refer to the directions parallel and perpendicular to the polarization direction, respectively. For small energies  $|\mathbf{p}^2/2| \ll U_p$ , we have that  $t_s$  is close to  $t_0$ , where  $t_0$  is one of the zeros of the vector potential,  $\mathbf{A}(t_0) = 0$ ; this can be seen from the equation for  $A(t_s)$ . The goal is to write an expansion of quantities of interest (such as the semiclassical action  $S(0, t) = \int_0^t dt' [\mathbf{p} + \mathbf{A}(t')]^2/2 + I_p t$ ) for small electron energies. This can be accomplished by expanding the time derivative of the action around  $t_0$ , up to a second-order term proportional to the small quantity  $(t_s - t_0)^2$ . By solving the approximate equation for the saddle time  $t_s$  and replacing it in the expression of the action, one obtains:

$$S(0, t_s) = S(0, t_0) + \frac{p_{\parallel}}{E(t_0)} \left( I_p + \frac{p^2 + 2p_{\perp}^2}{6} \right) + i \frac{(2I_p + p_{\perp}^2)^{3/2}}{3|E(t_0)|} + \dots \quad (6.7)$$

Consider now a pair of saddles: denoting the two saddle times in the pair by  $t_{s1}$  and  $t_{s2}$ , then, from Eq. (6.7) one obtains the following expression for  $S_2 - S_1 \equiv S(0, t_{s2}) - S(0, t_{s1})$ :

$$S_2 - S_1 = S(t_{01}, t_{02}) + p_{\parallel} \left( I_p + \frac{p^2 + 2p_{\perp}^2}{6} \right) \left[ \frac{1}{E(t_{02})} - \frac{1}{E(t_{01})} \right], \quad (6.8)$$

where  $S(t_{01}, t_{02}) \equiv \int_{t_{01}}^{t_{02}} \{[\mathbf{p} + \mathbf{A}(t')]^2/2 + I_p\} dt'$ . The expression obtained for the phase difference of a pair of saddles applies only for low momenta of the ejected electron. The reason for using the times  $t_{01}$  and  $t_{02}$  is that they do not depend on  $\mathbf{p}$ , making the analysis possible. The phase difference is seen to depend on the angle of ejection, via the quantity  $p_{\parallel}$ , only through the term  $\int_{t_{01}}^{t_{02}} A(t) dt$  and another one proportional to the difference  $E(t_{02}) - E(t_{01})$ . When doing the integration over the angles to obtain the angle-integrated ATI spectrum, the contribution of a certain saddle pair averages to zero if the corresponding phase difference of the pair depends on the angle. Hence, to avoid the cancellation of a certain pair, the necessary condition is to have  $\int_{t_{01}}^{t_{02}} A(t) dt = 0$  together with  $E(t_{02}) = E(t_{01})$ . If there is not at least one such a pair whose amplitude  $a_l a_m$  is not negligible, then one would expect a relatively flat angle-integrated ATI spectrum. Moreover, for a pair ( $lm$ ) whose phase difference does not depend on the angle of emission, the LATI peaks coming from the pair's interference occur at energies given by the condition  $S_l - S_m = 2N\pi$ , when constructive interference takes place between the contributions of the two saddles. These peaks are not affected by the angle integration.

To exemplify, we study in the next Subsection the case of a four-cycle symmetrical electric field, for which the interference occurs typically between a pair of saddles and an isolated saddle. We prove that, when integrating over the emission angle, the modulus squared of the total contribution is equal approximately to the modulus squared of the contribution coming from the saddle pair and the modulus squared of the isolated saddle contribution. This is in agreement with the previous discussion. The case of an anti-symmetrical electric field is presented in Subsection 6.7.2.

### 6.7.1 The case of symmetrical electric field

Let us consider the case when the electric field has the same value for both saddles,  $E(t_{01}) = E(t_{02})$ . This happens for example if the electric field is symmetrical with respect to the middle of the pulse [ $\phi = 0$  in Eq. (6.1)]. Fig. 6.10 shows such a possible configuration for a four-cycle  $\sin^2$  pulse; one can see that in this case  $t_{02} - t_{01} = 2\pi/\omega$ . Because of the strong nonlinear dependence of the ionization amplitude on the electric field, we discuss only the saddle pair with the highest electric field value. Then, from Eq. (6.8), using that the

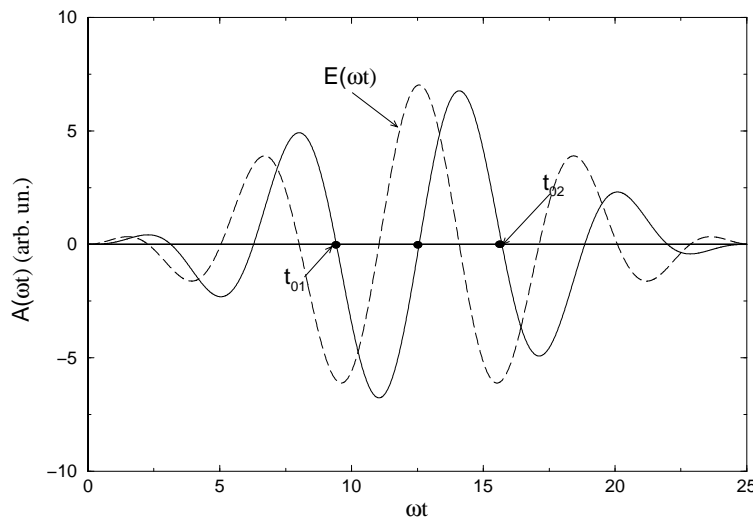


Figure 6.10: The case of a symmetrical electric field.

electric fields are equal at the two times  $t_{01}$  and  $t_{02}$  and that  $\int_{t_{01}}^{t_{02}} A(t') dt' = 0$  due to the asymmetry of  $A(t)$  with respect to the middle of the pulse, the condition for constructive interference for the saddle pair reads

$$\left(\frac{p_N^2}{2} + I_p\right) \frac{2\pi}{\omega} + \int_{t_{01}}^{t_{02}} A^2(t')/2 dt' = 2N\pi, \quad (6.9)$$

giving the energies of LATI peaks:  $p_N^2/2 = N\omega - [(\int_{t_{01}}^{t_{02}} A^2(t')/2 dt')/(2\pi/\omega) + I_p]$ . Thus, the pair has the property that its interference pattern does not depend on the angle of emission (see the previous general discussion at the beginning of this Section). The other possible pairs can be formed by the isolated saddle and  $t_{01}$  or  $t_{02}$ , respectively; these pairs are seen to depend on the

angle of emission, as the electric fields differ within each pair and also  $\int A(t)dt$  is non-zero between the pair's saddles [see Eq. (6.8)]. As a consequence, their interference patterns does not contribute to the angle-integrated spectrum.

The symmetrical pair's interference peaks are separated by  $\omega$ , the carrier wave frequency. Their energies are seen not to depend on the emission angle  $\theta$  and this explains why the LATI peaks are still well resolved after integrating over  $\theta$ . An illustration of this was presented in the left panel of Fig. 6.7, from Section 6.6. The expression for LATI energies is identical to the definition of the ATI peaks for a stationary field (the conservation of energy condition). With  $t_{01}$  and  $t_{02}$  taken as the beginning and the end of one optical cycle, the quantity  $\left(\int_{t_{01}}^{t_{02}} dt' A^2(t')/2\right)/(2\pi/\omega)$  resembles the definition of the ponderomotive energy  $U_p$ , for a stationary field.

As an application of the LATI energies formula, Figure 6.11 shows angle-resolved ATI energy spectra for a four-cycle pulse; the contribution is only that of the symmetrical pair's. Three different emission angles with respect to the polarization axis are depicted. Note the decrease of the ionization amplitude with increasing emission angle. The filled circles represent the LATI energies calculated from Eq. (6.9). The agreement is very good and indicates also that our expansion holds for not so small kinetic energies (in this case, up to  $0.15U_p$ ).

Furthermore, interesting effects could appear. This is due on one hand to the fact that LATI peaks do not depend on emission angle and on the other hand to the fact that the main contribution to the ionization amplitude comes from an isolated saddle point (corresponding to electron emission close to the middle of the pulse – see Fig. 6.10) and from one pair of saddles. The magnitude of the isolated contribution is the biggest, as the electron is emitted close to the peak of the electric field. If the pair's contribution is smaller, then, as a result, the angle-integrated spectrum will display a series of LATI peaks modulated by the saddle pair, superimposed over a background whose magnitude is given by the isolated saddle.

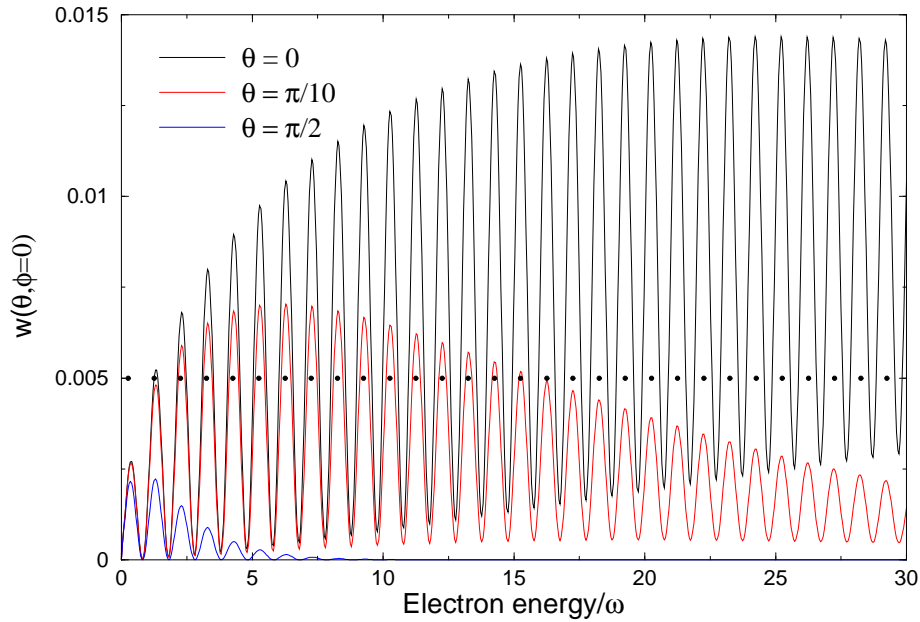


Figure 6.11: Angle-resolved ATI energy spectra at different emission angles for a  $\text{He}^+$  irradiated by a  $\sin^2$  pulse with  $E_0 = 0.4$  a.u. and field phase  $\phi = 0$ . The wavelength is 800 nm. Only the contribution of the symmetrical pair of saddles is shown. The filled circles represent the predicted LATI peaks, from Eq. (6.9).

Figure 6.12 shows the angle-integrated ATI spectrum for the case of a four-cycle symmetrical electric field. In agreement with those discussed above, the main contribution to the ionization rate comes from an isolated saddle (with the biggest magnitude) and from a pair of saddle points (responsible for the interference pattern in the angle-integrated spectrum). The second pair's contribution is six orders of magnitude lower than the first pair's. One can see that the magnitude of the LATI peaks is set by the isolated contribution, while the modulation of the spectrum is due to the pair of saddles. The peak separation in energy is equal to approximately  $\omega$ , the carrier wave frequency.

As discussed in Section 6.7, the ATI spectrum for each angle of emission consists of peaks at energies which do not depend on the angle (the LATI peaks are given by the interference of the saddles in the pair). The energy-resolved spectra for different emission angles are modulated by a factor depending on the angle, coming from the interference of each of the saddles in the pair with

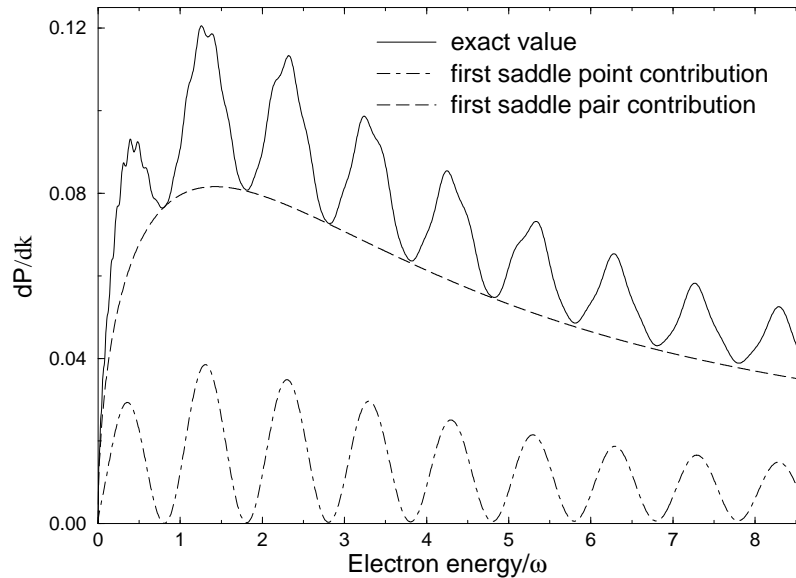


Figure 6.12: The saddle point contributions to the ionization probability of  $\text{He}^+$ , for a 4-cycle  $\sin^2$  pulse with symmetrical electric field. The pulse has 800 nm wavelength and the peak electric field is  $E_0 = 0.4$  a.u.

the isolated saddle. In the final angle-integrated spectrum, these fast oscillations depending on the angle average out, and one sees only the peaks at the angle-independent energies.

Increasing the pulse duration and/or intensity will result in better resolution for LATI peaks in the angle-integrated spectrum. Of course, if the pulse duration is too long, the effects just discussed become less relevant, as the pulse resembles a stationary field, where the carrier phase is no longer important in the physical processes. These aspects are discussed in the Section 6.8.

### 6.7.2 The case of anti-symmetrical electric field

For an anti-symmetrical electric field we have  $E(t_{01}) = -E(t_{02})$  and  $t_{02} - t_{01} = \pi/\omega$ . Figure 6.13 shows the first two saddle pairs. Due to the lower electric field magnitude, the second saddle pair (filled red circles) does not contribute

to the ionization amplitude. Equation (6.8) can be re-written as

$$\left(\frac{p^2}{2} + I_p\right) \frac{\pi}{\omega} + p_{\parallel} \left[ \int_{t_{01}}^{t_{02}} A(t') dt' + \left(I_p + \frac{p^2 + 2p_{\perp}^2}{6}\right) \frac{2}{E(t_{01})} \right] + \int_{t_{01}}^{t_{02}} \frac{A^2(t)}{2} dt = 2N\pi. \quad (6.10)$$

The situation is different from the symmetrical case, as because of the ' $p_{\parallel}$ ' term

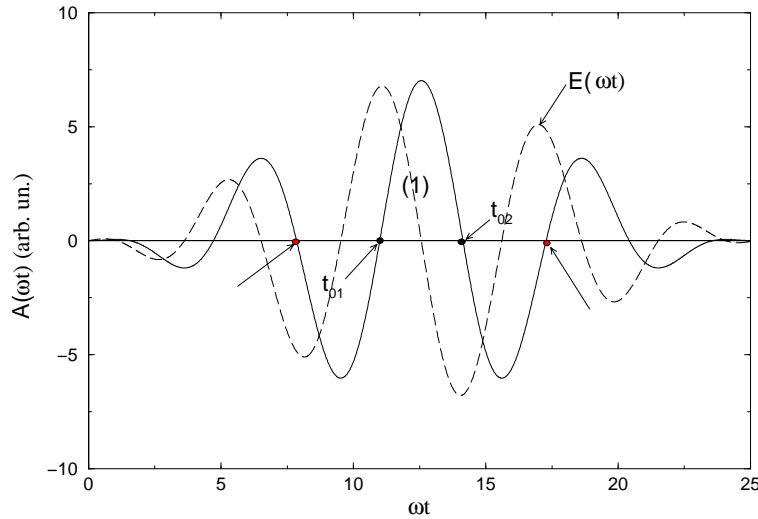


Figure 6.13: The case of an anti-symmetrical electric field.

in Eq. (6.10), the LATI peaks depend now on the emission angle. Their energies satisfy a cubic equation in  $p_N$  and the spacing between two consecutive peaks is no longer equal to the carrier frequency  $\omega$ , as in the case of the symmetrical electric field. Figure 6.14 shows the accuracy of the LATI peaks prediction formula.

The particularity of the anti-symmetrical case is that the dependence of LATI peaks on the emission angle relates to the quantity  $\int_{t_{01}}^{t_{02}} A(t') dt'$  (the region '(1)' in Fig. 6.13). The smaller its value is, the weaker the dependence on the emission angle. A typical example was given in left panel of Figure 6.8, Section 6.6. The angle-integrated spectrum in the right panel shows no peaks: as the position of the LATI peaks depends on angle, the integration results in a relatively smooth angle-integrated spectrum (right panel in the same figure).

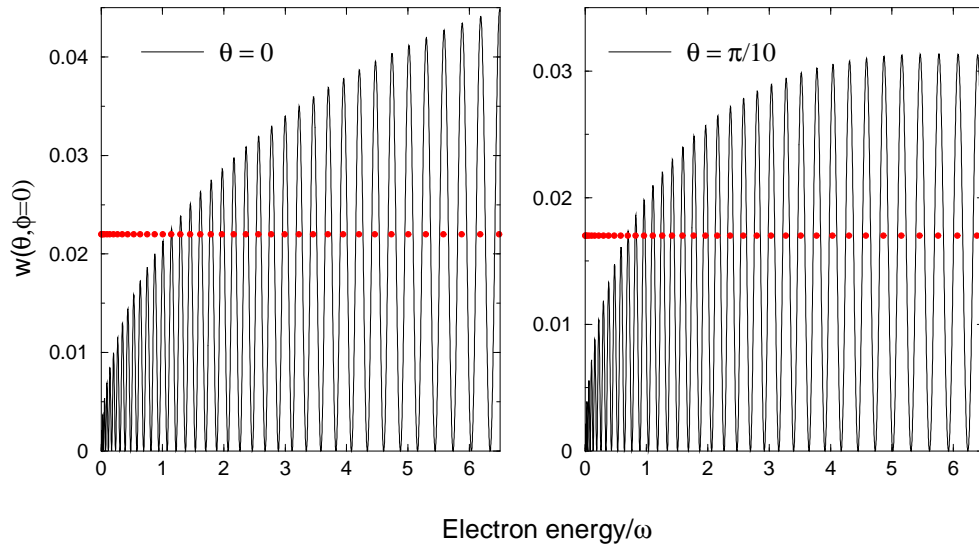


Figure 6.14: Angle-resolved LATI energy spectra. Only the contribution of the first pair is shown. The parameters are the same as in Fig. 6.11, only the electric field is anti-symmetrical:  $\phi = \pi/2$ . The filled circles are the predicted LATI peaks, from Eq. (6.10). The emission is along the polarization direction (left panel) and at an angle  $\theta = \pi/10$  with respect to the polarization axis (right panel).

## 6.8 Influence of pulse parameters on direct ionization

For a given intensity, there is a maximal pulse duration for which phase effects still play a role, as the previous discussions suggest. Moreover, we show that the resolution of LATI peaks depend on the pulse intensity, duration and shape.

### 6.8.1 Influence of the field phase

From the previous sections, we have seen that LATI peaks depend on the field phase value. We choose here a four-cycle  $\sin^2$  pulse and study the angle-integrated LATI spectrum while changing the field phase.

To see how sensitive the effect of LATI disappearance is with the phase variation from zero, Fig. 6.15 shows calculations done for increasing phases. The spectra for nonzero phase have no LATI peaks, and the effect is visible even

for phases as small as  $\pi/10$  (the blue curve). For the anti-symmetrical electric

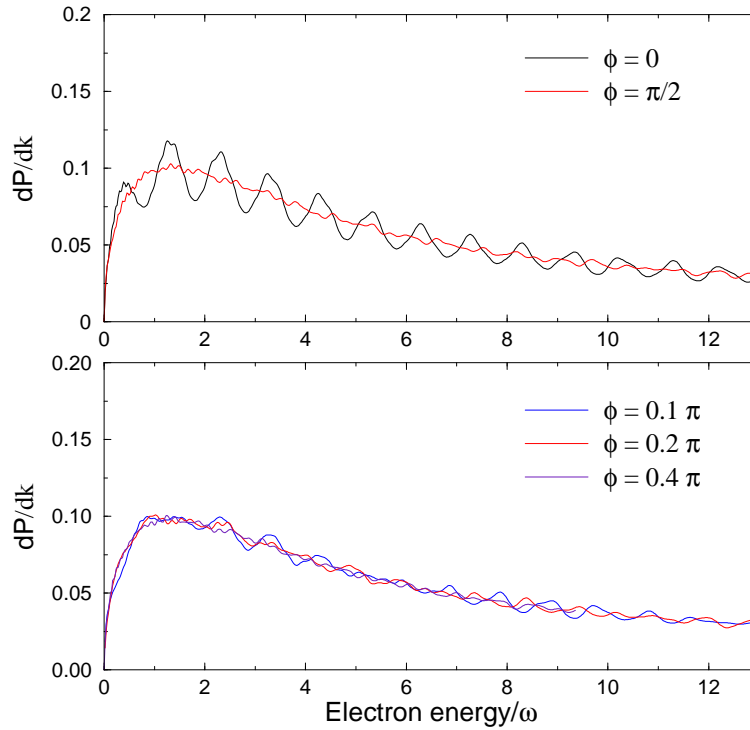


Figure 6.15: The angle-integrated ionization probability in  $\text{He}^+$  for the same pulse as in Fig. 6.12, only for various field phases.

field ( $\phi = \pi/2$ ), the spectrum is almost flat, with no structure.

### 6.8.2 Influence of the intensity

For short pulses and/or low intensities, the contribution to the ionization amplitude of the saddle pair is much less than the magnitude of the isolated saddle. Under such conditions, even for a symmetrical electric field, the LATI interference pattern has little contrast or is even absent in the angle-integrated spectrum. The left panel in Fig. 6.16 shows a case where despite the phase being zero, the LATI do not appear in the spectrum. The explanation is that the amplitude of the saddle pair's contribution is so low that does not influence the ATI spectrum. To improve the contrast, it suffices to increase the intensity (see the centre panel). This way, the contribution of the saddle pair

increases and LATI become better resolved. Further increase of the intensity allows higher energy peaks to gain resolution (right panel).

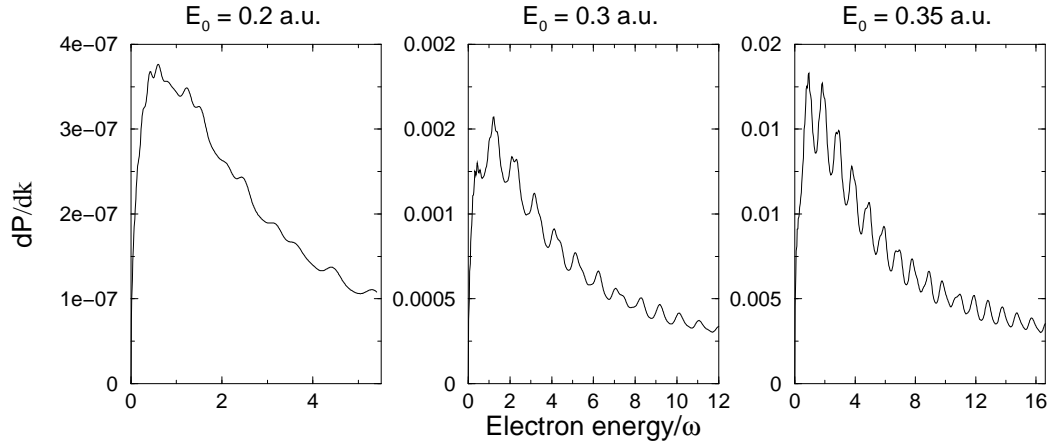


Figure 6.16: Angle-integrated ionization probability of  $\text{He}^+$  for increasing intensity. The electric field is symmetrical with respect to the middle of the pulse. The rest of the pulse parameters are the same as in Fig. 6.18.

If we increase the intensity for a field with non-zero phase, the ATI spectrum changes as in Fig. 6.17. The spectrum remains relatively flat, with no well-resolved ATI peaks.

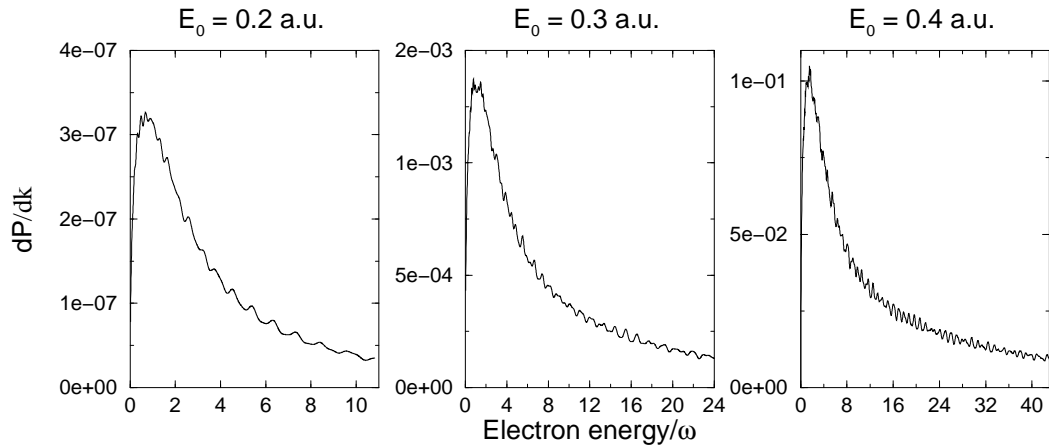


Figure 6.17: Angle-integrated ionization probability of  $\text{He}^+$  for increasing intensity. The electric field has the phase  $\phi = \pi/4$ . The rest of the pulse parameters are the same as in Fig. 6.18.

### 6.8.3 Influence of pulse duration

For a short pulse, we have seen that the carrier phase can influence to a great extent the appearance of the LATI peaks in the angle-integrated ATI spectra. For phases different from zero, the LATI peaks are less and less resolved, until they eventually disappear. In addition, even for a symmetrical electric field, if the intensity is too low and/or the pulse is too short, the LATI peaks are not well resolved.

A possible way to have better contrast for the LATI peaks is to increase the pulse duration. Figure 6.18 shows a field with zero phase, which should have LATI peaks in the angle-integrated spectrum. For a pulse as short as two cycles and low intensity, the magnitude of the saddle pair contribution to the ionization spectrum is much lower than that of the isolated saddle. Hence, there is no modulation in the spectrum and the LATI peaks are absent. Because the relative magnitude of the isolated saddle contribution to that of the saddle pair is set by the ratio of the ionization rates at the corresponding birth times, its variation is more abrupt in the region of low electric fields. This is because the tunneling ionization rate varies strongly at low electric fields. By increasing the pulse duration, the contribution of the saddle pair increases relatively to the isolated saddle contribution, and the LATI peaks begin to appear, separated approximatively by  $\omega$ , the carrier wave frequency.

If the pulse is long enough, the phase effects become less important (see also Ref. [32] for phase effects related to ionization in circularly polarized short pulses, where the authors reached similar conclusions). Figure 6.19 shows the angle-integrated spectra for a non-zero field phase. For a four-cycle pulse, the LATI are not well resolved, as expected (see the left panel). The centre panel displays the results for longer pulses (five and six optical cycles). Despite the non-zero phase value, LATI peaks are seen in the spectra and the lower their energy, the better the resolution. Increasing the pulse duration, the resolution improves even more, looking similarly to the ATI spectrum for a stationary

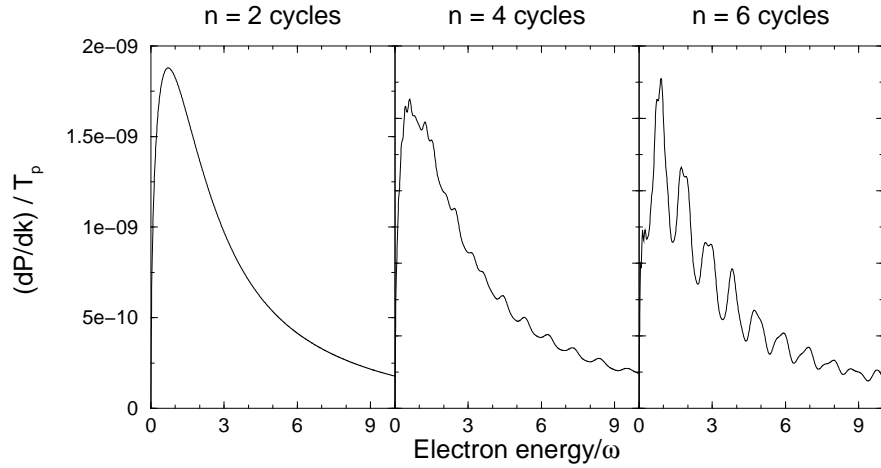


Figure 6.18: Angle-integrated ionization probability per pulse duration in  $\text{He}^+$  irradiated by a 4-cycle  $\sin^2$  pulse with  $E_0 = 0.2$  a.u. and  $\phi = 0$ .

field. The spacing between the peaks is approximately  $\omega$ , the carrier wave frequency. The explanation for this is that with increasing duration, the field

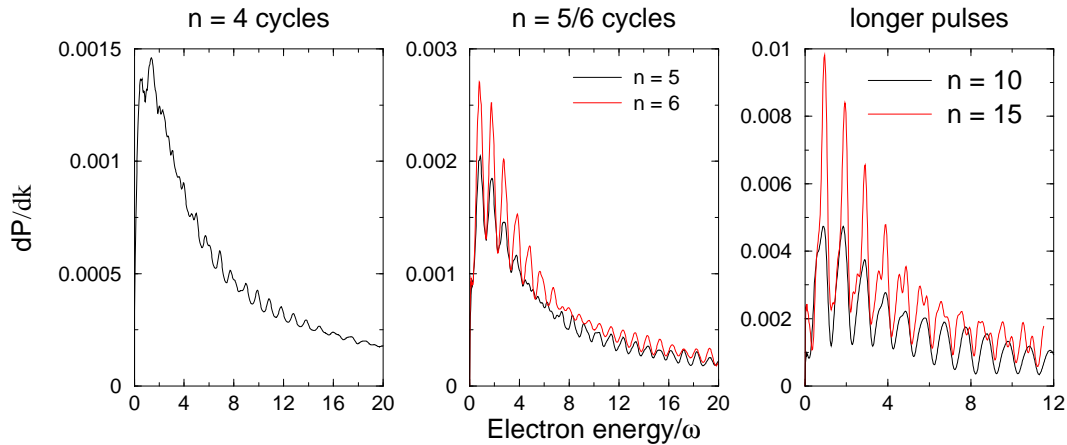


Figure 6.19: Angle-integrated ionization probability in  $\text{He}^+$  for different duration  $\sin^2$  pulses with  $E_0 = 0.3$  a.u. and phase  $\phi = 0.23$  rad. The rest of the parameters are the same as in Fig. 6.18.

near the peak of the envelope (where the main contribution to the ionization amplitude comes from) encompasses a large number of optical cycles. This in turn, resembles a stationary field. The larger the pulse duration is, the less relevant the phase effects become. For the intensity used in Fig. 6.19, already for nine cycles and longer, the phase effects diminish when compared to a

four-cycle pulse.

In conclusion, for a given intensity, one possible way to increase the resolution of LATI peaks is to increase the pulse duration. However, a pulse that is too long loses the sensitivity to the phase effects. For symmetrical electric field and same pulse duration, better resolution can be achieved by increasing the field intensity.

#### 6.8.4 Influence of the binding energy and pulse shape

The pulse shape can affect the ATI spectrum due to effects induced by the shape of the envelope (more precisely, the envelope variation near its peak).

Figure 6.20 shows the angle-integrated ATI spectrum for a sech pulse [for definition, see Eq. (6.2)]. The spectrum for symmetrical electric field is compared to the one for the case of a  $\sin^2$  pulse, with the same FWHM (in amplitude). In the left panel it can be seen that the general effect of interference described previously is still present, independent of the pulse shape. The right panel presents the situation for different field phases, where the LATI are less resolved.

Another case we choose to study is a Gaussian pulse, with the width such that its FWHM (in amplitude) is the same as for a four-cycle  $\sin^2$  pulse. The same comparison as for the sech pulse is done. Figure 6.21 shows in the left panel that the general behavior of LATI peaks contrast with the field phase is the same. The right panel depicts the LATI losing resolution for phases different from zero.

Both the sech and Gaussian pulse calculations prove that the analysis done in Section 6.7 applies to an arbitrary pulse shape.

One other effect appears, and it is due to the form of the field envelope near its peak. In Fig. 6.21, the LATI peaks for the Gaussian pulse appear to have a better contrast than those for the sech pulse in Figure 6.20. This underlines

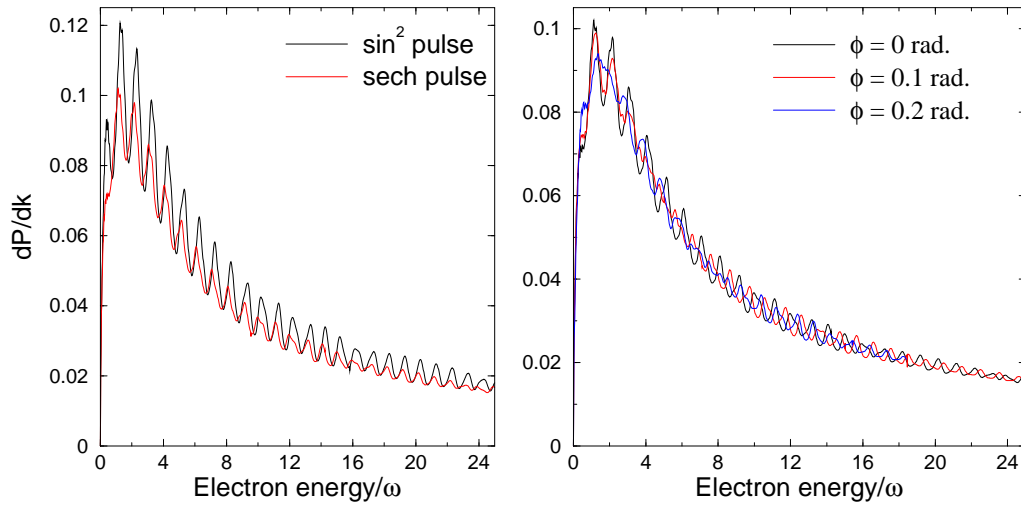


Figure 6.20: Left panel: angle-integrated ionization probabilities for  $\text{He}^+$  in a 800 nm, 4-cycle  $\sin^2$  pulse and a sech pulse with identical FWHM (in amplitude). The peak electric field is  $E_0 = 0.4$  a.u. The phase is  $\phi = 0$ . Right panel: the probability for different pulse phases for the sech pulse.

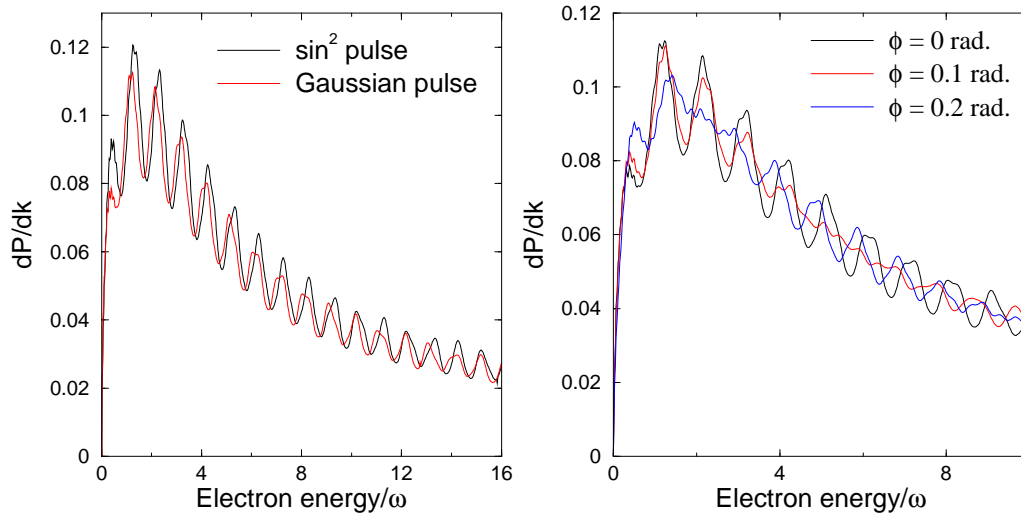


Figure 6.21: The same as in Fig. 6.20, but for a Gaussian pulse.

the influence of the field envelope: because the sech pulse has a faster decrease in amplitude near the peak of the envelope, the contribution of the saddle pair is smaller than for the case of a  $\sin^2$  or Gaussian field. As a consequence, the LATI become less resolved from the background. The Gaussian pulse results agree better to the results obtained for the  $\sin^2$  pulse. The reason is that the the two envelopes are nearly identical to the peak, provided they have the

same FWHM (in amplitude).

To conclude, we present results for the helium atom ( $I_p = 0.903$  a.u.). Figure 6.22 (left panel) presents angle-integrated ATI spectra for a  $\sin^2$  pulse and a sech pulse, with the same FWHM (in amplitude).

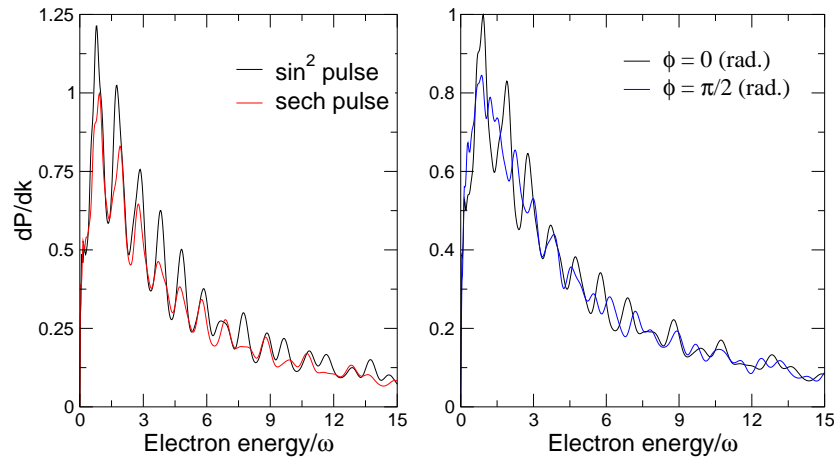


Figure 6.22: The same as in Fig. 6.20, but for helium, at intensity  $I = 1 \times 10^{15}$  W/cm<sup>2</sup>. (The Keldysh parameter  $\gamma = 0.45$ .)

Due to the lower ionization potential and the low intensity (where the ionization rates vary rapidly with the electric field amplitude), the effect of the envelope on the ATI spectrum is stronger than in the case of the He<sup>+</sup> ion (see Figure 6.20). The right panel of Fig. 6.22 shows the angle-integrated spectra for two different field phases (namely for the case of the symmetrical and anti-symmetrical electric pulse). For the case of the anti-symmetrical electric field, the ATI spectrum is not flat, as expected; because of the low intensity, the asymmetry effects are not strong enough. To increase the intensity for this case would mean to approach the saturation intensity.

## 6.9 Field-phase dependence of emission asymmetry

Depending on the phase of the laser field, the emission of ionized electrons can occur in the positive direction of the polarization axis with different probability than in the negative direction. To assess the importance of the phase effects in the emission of electrons in the positive/negative direction we define the asymmetry:

$$R = \frac{P_+ - P_-}{P_+ + P_-}, \quad (6.11)$$

where  $P_+$  is the total probability of emission in the positive direction of the polarization axis and  $P_-$  is the total probability in the negative direction. The

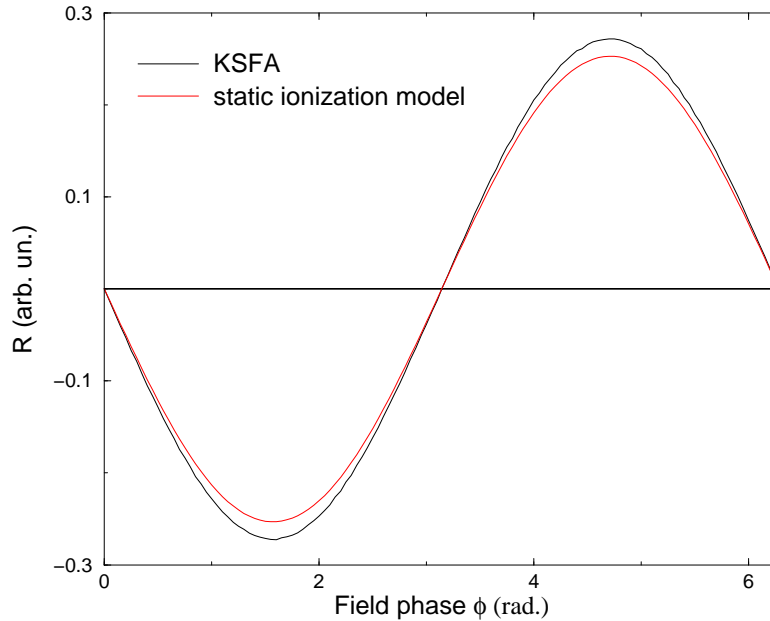


Figure 6.23: The asymmetry for direct ionization in  $\text{He}^+$  for a peak electric field  $E_0 = 0.4$  a.u., at a wavelength of 800 nm. The field is a  $\sin^2$  field, encompassing four optical cycles. The two curves show the KSFA results and the prediction of a simple model based on the exact ionization rates in a static electric field.

emission probabilities are calculated using the KSFA model, by integrating over the energy of the ejected electron and over the emission angles corresponding to emission in the positive and negative direction, respectively. The black curve

in Figure 6.23 shows the variation of  $R$  with the field phase. Its variation is similar to a sinusoidal dependence and it reaches zero for phases  $\phi = 0$  and  $\phi = \pi$ , when the vector potential  $\mathbf{A}(t)$  is anti-symmetrical with respect to the middle of the pulse (thus, the electrons are emitted with the same probability in the positive/negative direction of the polarization axis).

From the Simpleman's model, at a time  $t_0$  during the pulse, the electron is born in the continuum with a momentum along the polarization axis  $p_1 = -A(t_0)$ . The probability of emission depends exponentially on the modulus of the electric field  $|E(t_0)|$ . For a  $\sin^2$  pulse, we have that  $A(t, \phi) = -A(t, \pi + \phi)$  ( $\phi$  is the field phase) and the same for the electric field. Therefore, by changing the phase with  $\pi$ , the emission of electrons changes direction. This explains why the asymmetry factor  $R$  in Figure 6.23 satisfies  $R(\phi + \pi) = -R(\phi)$ .

Starting from the Simpleman's model, we can calculate the total probabilities of emission in the positive/negative direction of the polarization axis as:

$$\begin{aligned} P_+ &= \int_0^{T_p} \Gamma_+(|E(t')|) dt' \\ P_- &= \int_0^{T_p} \Gamma_-(|E(t')|) dt'. \end{aligned} \quad (6.12)$$

In Eqs. (6.12), we assume that the depletion is negligible [i.e.,  $\int_0^t \Gamma(|E(t')|) dt' \ll 1$  at all times]. We define the ionization rate  $\Gamma_+(|E(t)|)$  as being equal to the exact ionization rate in the static electric field of magnitude  $|E(t)|$  if  $A(t) < 0$ , and zero if  $A(t) > 0$ . The latter condition ensures that the emission occurs in the positive direction:  $p_1 = -A(t) > 0$ . A similar definition is adopted for  $\Gamma_-(|E(t)|)$ , only the condition for emission in the negative direction reads  $A(t) > 0$ , such that  $p_1 = -A(t) < 0$ . The results are shown by the red curve in Fig. 6.23. They are in good agreement with the KSFA results which suggests that for the frequency and intensity used here, the ionization process can be approximated as adiabatic and occurs via tunneling.

A similar curve for the asymmetry factor  $R$  has been obtained in the work of Chelkowski, Bandrauk and Apolonski [99], based on *ab initio* calculations.

Their curve has an offset with a certain phase, so  $R(\phi = 0) \neq 0$ . This may be attributed to the Coulomb effects, which are only partially included in the KSFA model.

## 6.10 Comparison with *ab initio* results

In this section, we compare predictions of the KSFA model with exact results<sup>1</sup>, aiming at establishing the differences between the two calculations. A possible way to improve this agreement is suggested.

The usual SFA model doesn't take into account the Coulomb interaction of the electron with the atomic core. The only place where the Coulomb interaction is taken into account is in the ground state used in the SFA amplitude. This ground state is the exact ground state of an electron bound by a Coulomb potential. The Krainov Coulomb-corrected SFA accounts for the influence of the Coulomb potential in the tunneling step of the ionizing electron; it reduces to a factor proportional to the Coulomb potential that multiplies the Volkov solution describing the final wavefunction of the electron. What it still uncorrected for the Coulomb interaction is the motion of the electron in the continuum. The reason is that due to the large electric field, the electron spends little time in the vicinity of the atomic core. The electron's large excursion amplitudes under the influence of the laser field only justifies neglecting the Coulomb interaction.

To assess the main differences between the Coulomb-corrected SFA and the exact results, we study some ATI spectra for two cases. Figure 6.24 shows the emission spectrum for an electron ejected at an angle  $\theta = 10^\circ$  with the polarization axis, for a two-cycle pulse. The KSFA results agree quantitatively well with the results obtained from the integration of the Schrödinger equation. One should remember that the usual SFA model gives results that are

---

<sup>1</sup>The author thanks Dr. R M Potvliege for the *ab initio* results, obtained using a numerical code courtesy of Dr. B Piraux.

consistently lower than those given by KSFA. Also, the ATI peaks energies as coming from the KSFA are slightly shifted in energy with respect to the exact results. The energy shift seems to increase with increasing electron energy.

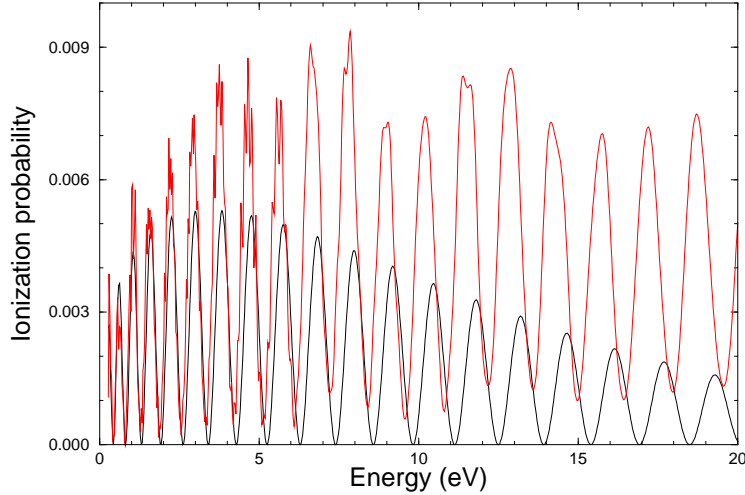


Figure 6.24: The ionization probability for an ejection angle  $\theta = 10^\circ$  with respect to the polarization direction for a  $\text{He}^+$  ion irradiated by a two-cycle  $\sin^2$  pulse, with  $\phi = \pi/2$ . The intensity is  $10^{16} \text{ W/cm}^2$  and the carrier wavelength is 400 nm. The red curve gives the *ab initio* results and the black curve the KSFA results.

Figure 6.25 shows the same as Figure 6.24, only for a longer pulse (four cycles). The general conclusions hold: the positions of the ATI peaks are energy-shifted, and the KSFA peaks show less structure than the exact peaks, obtained from the integration of the Schrödinger equation. Qualitatively, the number of ATI peaks is the same, only their energy differs from the exact value and the structure is less complicated.

Comparing to the exact spectra, one can say that the KSFA model is satisfactory to some extent, but there are differences in the structure of the ATI peaks and a small shift in ATI peak-energy is present. Better agreement is expected for higher laser intensities, or at least smaller frequencies. The comparison is hampered for the high intensity regime by a lack of data for the exact results. This is due to the increased numerical difficulty in solving the Schrödinger equation.

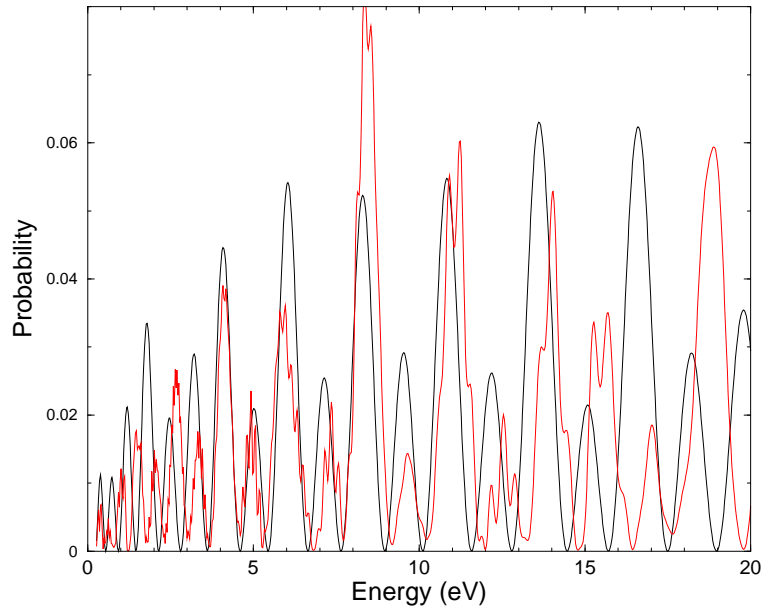


Figure 6.25: The ionization probability for an ejection angle  $\theta = 10^\circ$  with respect to the polarization direction for a  $\text{He}^+$  ion irradiated by a four-cycle  $\sin^2$  pulse, with  $\phi = \pi/2$ . The intensity is  $10^{16} \text{ W/cm}^2$  and the carrier wavelength is 400 nm. The red curve gives the *ab initio* results and the black curve the KSFA results.

The shift in the positions of the LATI peaks could be attributed to the bigger influence of the Coulomb interaction on the electron trajectories with the same final (low) momentum state. Some of the electron wavepackets created after tunneling through the potential barrier are ‘direct’, in the sense that after emission they propagate away from the atomic core. Other trajectories (presumably corresponding to the ‘indirect wavepackets’ of Ref. [4]) remain in the vicinity of the nucleus for a longer time; for these we expect the Coulomb interaction during the motion of the electron in the continuum, which is not included in the SFA model, to play a more important role .

A more detailed and complete comparison is presented in Figure 6.26: the density of probability in the momentum space<sup>2</sup> as obtained from the fully numerical solution of the Schrödinger equation is compared to the predictions of the KSFA model. This case differs from the ones studied so far in that the

<sup>2</sup>Courtesy of Dr. Bernard Piroux, from A. de Bohan, “Thèse de Doctorat”, Université Catholique de Louvain, 2001

ponderomotive energy is actually *smaller* than the binding energy ( $U_p = 0.29$  and  $I_p = 0.5$  atomic units, respectively). In this regime, it is expected that many electron trajectories will stay close to the atomic core, before leaving it, probably experiencing many interactions with the core [57], which agrees with the observation about the existence of the ‘indirect wavepackets’ of de Bohan *et al.* in Ref. [4]. Within the rescattering SFA model (using the atomic potential as expansion parameter), calculations done in Ref. [57] show that for the case  $U_p < I_p$ , the first-order term, or rescattering, is much larger than the zeroth-order term (which, Coulomb-corrected, gives the KSFA). This may indicate, according to [57] that the perturbation expansion in terms of the atomic potential actually breaks down, or converges more slowly. The Keldysh adiabaticity parameter  $\gamma \approx 1$ , so we are at the borderline between the tunneling and the multiphoton regime. In the *ab initio* calculation, the ATI peaks are much better defined than in the SFA model and the momentum distribution extends to slightly higher momentum values. Also, the up-down asymmetry along the polarization axis Oz is obvious, while the SFA gives a symmetrical distribution. So, the symmetry breaking could be attributed to effects related to the Coulomb interaction.

In the same figure, the comparison made in the upper picture with the results of a semiclassical approximation refers to an earlier version of the SFA, due to Faisal [63] and Reiss [64]. In the lower picture, we show the results of the KSFA model, for which an overall qualitative agreement can be seen. For the comparison to be more relevant, it requires a higher intensity case (where SFA is expected to be more accurate). At the same time, the numerical difficulty of the *ab initio* calculations increases considerably.

A last comparison is made for 4-cycle,  $\sin^2$  pulse, at an intensity  $I = 10^{16}$  W/cm<sup>2</sup>, at 400 nm. We compare the *ab initio* results to the predictions of the KSFA model for a symmetrical (Figure 6.27) and anti-symmetrical pulse (Figure 6.28). The interference effect is visible in the *ab initio* calculation, but it is less obvious than in the KSFA calculation. This may be due to the shorter

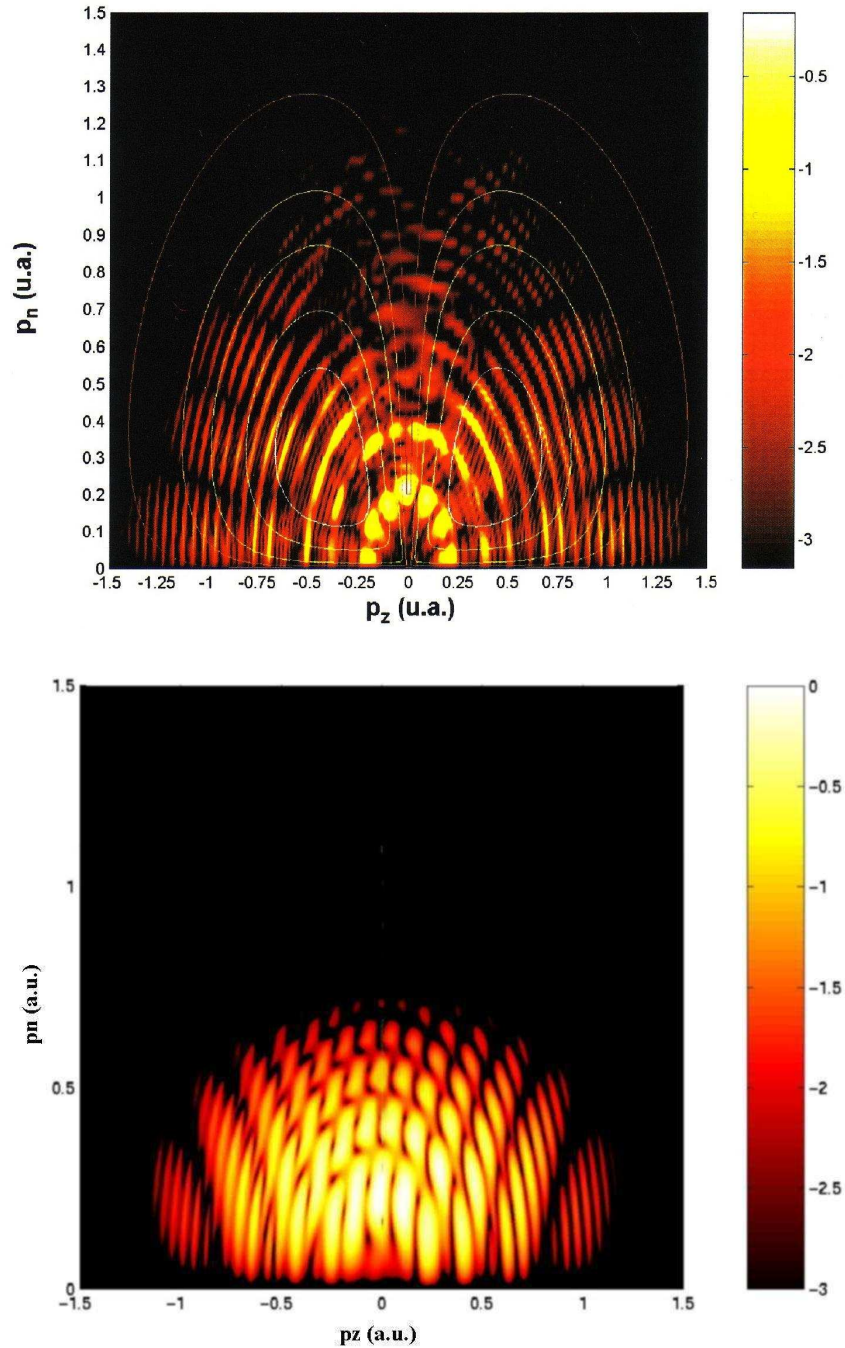


Figure 6.26: Emission probability in hydrogen, for ejection of the electron along the polarization axis with momentum  $p_z$  and in the perpendicular plane with momentum  $p_n$ . The laser has a peak intensity of  $1.3 \times 10^{14}$  W/cm<sup>2</sup>, eight optical cycles and the wavelength is 800 nm. The electric field is symmetrical with respect to the middle of the pulse. The *ab initio* result is displayed in the upper panel [3], while the lower one shows the Coulomb-corrected SFA result. White lines in the top diagram are the predictions of the SFA in the velocity gauge [4].

wavelength of the field (half the value used in Section 6.8).

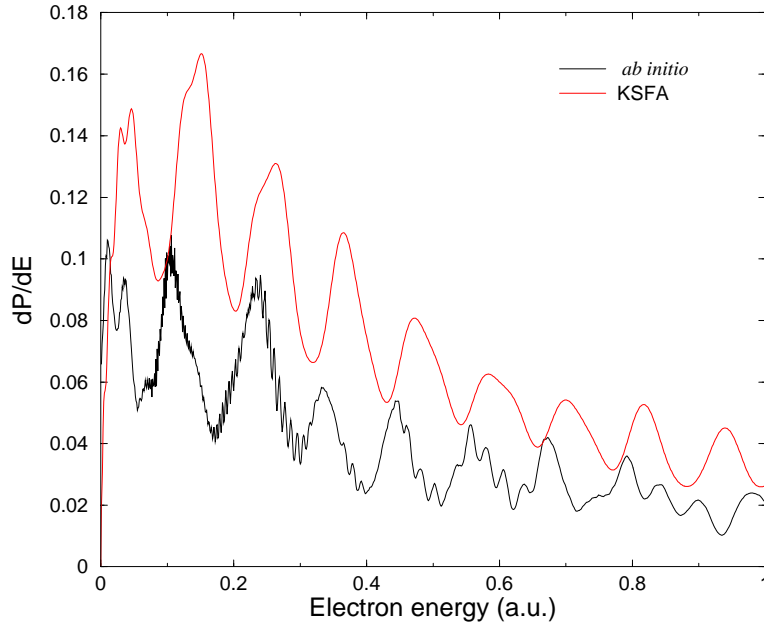


Figure 6.27: Angle-integrated ATI spectrum of  $\text{He}^+$  irradiated by a 400 nm, 4-cycle  $\sin^2$  laser pulse, with peak intensity of  $1 \times 10^{16} \text{ W/cm}^2$ . The field phase is  $\phi = 0$ . The *ab initio* result is compared to the KSFA result.

Based on the conclusions from this Section, it appears that the behavior of the ATI angle-integrated spectrum with the phase of the field described in Section 6.8 should remain valid.

## 6.11 Conclusions

In this chapter, we have presented predictions of the Krainov Coulomb-corrected SFA model (KSFA) for direct ionization in short laser pulses. The numerical results were obtained using the saddle point method. We showed that the agreement with the exact numerical results is excellent for the pulse parameters used.

The main point is the interference effect in the ATI spectrum and its dependence on the field phase. Only for a symmetrical electric field with respect to

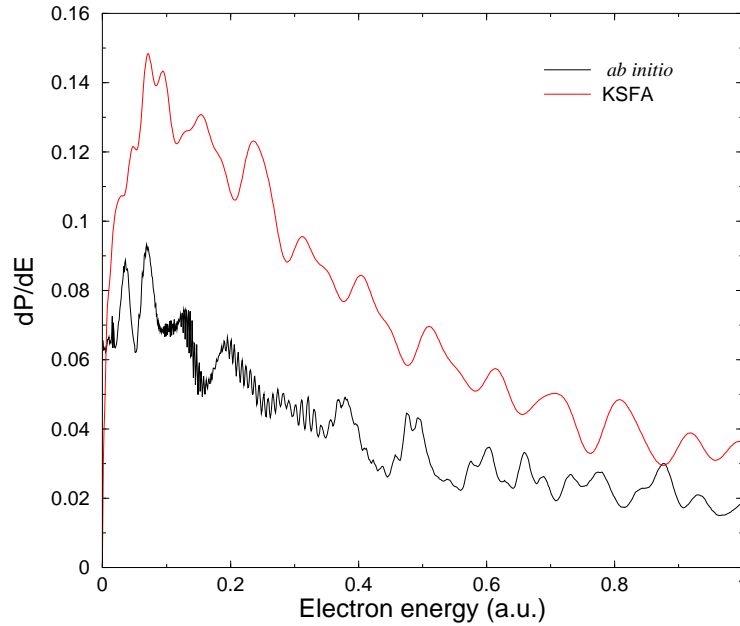


Figure 6.28: Comparison between the *ab initio* result and the KSFA result. The pulse parameters are the same as in Fig. 6.27, only the electric field is asymmetrical:  $\phi = \pi/2$ .

the middle of the pulse there are LATI peaks in the angle-integrated spectrum. Otherwise, the spectrum is flat for field phases departing from the zero value. This may suggest a way to measure the absolute phase of a short laser pulse.

The analysis of the influence of pulse parameters, as pulse duration and intensity, shows that the phase sensitivity of LATI manifests only for a small number of optical cycles. Increasing the pulse duration results in losing the phase effects, as the ATI spectrum begins to resemble the one for the stationary field.

We have also analyzed the total ionization probability and compared it to the results obtained from integration over the pulse duration of the exact ionization rates in static electric field. The agreement of the KSFA model is much better than for the usual SFA.

The last part of the chapter compares angle-resolved LATI spectra from the KSFA model to the exact results from the numerical integration of the Schrödinger

equation. We show that the agreement is good as order of magnitude, but there is a shift in the energies of the LATI and less structure of the peaks for the KSFA. The differences may originate in the neglect of the Coulomb interaction for the motion of the electron after tunneling. A more accurate SFA would have to incorporate these corrections for the motion of the electron in the continuum.